Solar Corona Amplitude Scintillation Modeling and Comparison to Measurements at X-Band and Ka-Band

D. Morabito[1]

Signal-strength fluctuations on a spacecraft-to-Earth link due to solar charged particles can degrade telemetry performance. The degree of amplitude scintillation induced on an emitted spacecraft signal by the intervening charged particles of the solar corona during a spacecraft-to-Earth superior conjunction depends on the minimum distance from the Sun of the signal ray path (solar elongation), the current phase of the solar cycle (solar maximum versus solar minimum), and the sub-solar latitude of the signal path. For spacecraft telemetry, frame errors have been observed to significantly increase due to scintillation, when the solar elongation becomes small enough, or when the solar coronal environment of the signal path is plagued with solar activity such as coronal mass ejections or streamers. This degradation in telemetry data return occurs at solar elongation angles of 2 deg and below at 8.4 GHz (X-band) and is expected to start occurring at about 1 deg at 32 GHz (Ka-band). This article presents both theoretical and statistical models, which have been derived based on spacecraft solar conjunction measurements to characterize the degree of solar scintillation as a function of solar elongation angle at both X-band and Ka-band. Such models may be useful to flight projects and design engineers in the planning of solar conjunction operational scenarios.

I. Solar Charged-Particle-Induced Scintillation on Signal Propagation

Signal-strength fluctuations on a spacecraft-to-Earth link can degrade received telemetry performance (see Fig. 1). The degree of amplitude scintillation induced on an emitted signal by the intervening charged particles of the solar corona during a spacecraft-to-Earth superior conjunction depends on a variety of factors. One important factor is the minimum distance from the Sun of the signal ray path ($r_{\min}$ in Fig. 1), usually measured in number of solar radii. If the signal path is close enough to the Sun, the solar elongation angle (1 solar radii = 0.26 deg) or Sun–Earth–probe (SEP) angle (SEP in Fig. 1) is sometimes used to express ray-path distance. As the electron-density fluctuations increase as the SEP angle decreases, the degree of amplitude (or intensity) scintillation increases until an SEP angle is reached in which the fluctuations saturate (that is, the rms of the fluctuations in intensity is comparable to the mean intensity).
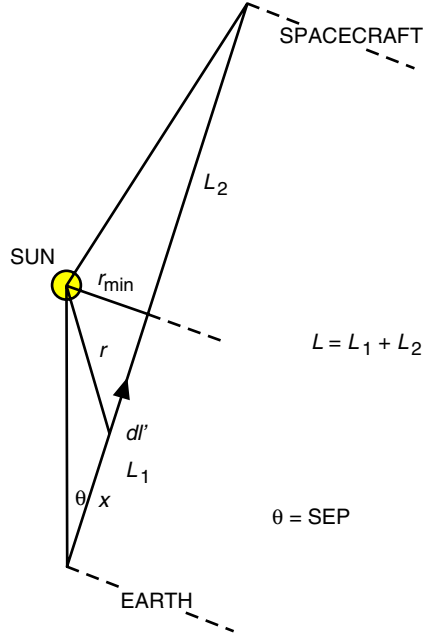

Fig. 1. Relevant solar conjunction geometry of the Earth and spacecraft relative to the Sun.

The phase of the solar cycle is another factor that can affect the degree of scintillation. Scintillation is expected to be worse during solar maximum conditions than during solar minimum conditions. During periods of solar maximum, there is a higher incidence of solar events and a higher likelihood that the signal path will be affected by the coronal density fluctuations. Such events include coronal mass ejections and the appearance of streamers. The sub-solar latitude of the signal path is another factor that can affect the degree of scintillation. There may be less activity in the polar (high) latitudes due to less-dense, less-turbulent media such as coronal holes. During solar maximum periods, transient coronal solar activity may occur in any sub-solar latitude of the signal path, while during solar minimum conditions coronal activity is more or less confined in the equatorial regions. Disentangling solar-latitude dependence and solar-activity dependence in each conjunction data set is difficult. In addition, many times the ingress and egress scintillation profile curves are asymmetric and could take on a different character depending on solar conditions. The degree of scatter in the amplitude measurements (scintillation) about a representative profile also can vary depending upon conditions.

The scintillation index is a measure of the degree of fluctuation that a signal's amplitude experiences due to passage through the small-scale plasma irregularities in the corona. It can be calculated from a measurement time series of signal strength as the ratio of the rms of the received power fluctuations relative to the mean power over the observation interval. The scintillation index, m, thus is defined as the rms of the received intensity fluctuations divided by the mean intensity, and it is sensitive only to characterizing the strength of small-scale (a blob size smaller than a Fresnel zone size) charged-particle density fluctuations. In the realm of weak scintillation ($0 < m < 0.5$), the rms of the fluctuations is small relative to the mean intensity. In the realm of strong scintillation, the rms of the fluctuations will be comparable to the mean intensity. As the SEP angle decreases, the scintillation index for a point source will increase until saturation occurs, and then there will not be any further increase in m as the SEP angle decreases. Saturation usually is reached at an SEP angle of $\sim$1.2 deg for 8.4 GHz (X-band) and $\sim$0.6 deg for 32 GHz (Ka-band). The time scale of the fluctuations will become shorter as the SEP angle decreases further in the realm of strong scintillation. The time resolution of the measurements will determine the fastest fluctuation time for which the measured scintillation index applies, while the period of the data used in the estimate determines the slowest fluctuation time.

For spacecraft telemetry, frame errors have been observed to significantly increase when the scintillation index reaches values of 0.3 and above [1]. Below a scintillation index of 0.3, few frame errors due to scintillation have been observed when sufficient margin was available in both the carrier and data channels. This transition point where telemetry frame errors significantly increase occurs near 2 deg for X-band and is expected to occur near $\sim$1 deg for Ka-band [1]. It is planned to test this with flight project telemetry data to be acquired during future solar conjunction experiments, such as with the Mars Reconnaissance Orbiter (MRO). Flight projects and design engineers thus can use such information in the planning of solar conjunction operational scenarios.

II. Solar Scintillation Measurement Data Sets

This section discusses the solar scintillation and spectral broadening measurements used to evaluate parameters in the theoretical and statistical models discussed later in Sections III and IV.

A. Description of the Measurements

The X-band and Ka-band scintillation index or relative power fluctuations [rms/mean P_c/N_o or signal-to-noise ratio (SNR)] were measured from recent solar conjunction experiments of interplanetary space-craft missions, which included Mars Global Surveyor (MGS) in May 1998 [2], Stardust in 2000 (X-band only), Cassini in May 2000 [3], Deep Space 1 (DS1) in October–November 2000 [4], and Cassini in June 2001. These data points are displayed in Fig. 2 for both X-band and Ka-band along with the theoretical model curves described in Section III. Most of the X-band data points from MGS 1998 were from Block V Receiver (BVR) closed-loop data, while most of the data points (X-band and Ka-band) from the Cassini solar conjunctions were estimated using a software phase-locked-loop (PLL) program run on open-loop-receiver sampled data recorded during the passes. In the region of strong scintillation, there is increased scatter of the data points about the model, predominately at X-band [SEP < 2 deg in Fig. 2(a)].

The PLL algorithm used on the open-loop data samples acquired during strong scintillation or saturation results in lost fluctuation information. This is because of filtering effects of the PLL when the signal SNR gets too low during the deep fading, which results in depressed estimates of the scintillation index. Therefore, the X-band scintillation data points with SEP < 1 deg were evaluated using an alternative approach. The histogram of the open-loop amplitude samples were fit to a Rician distribution function, solving for the Rician mean and sigma parameters, as well as a scale factor. These then were converted to scintillation index using appropriate formulation [5]. This approach appears to be very reasonable, as the resulting scintillation-index values lie near unity, as expected in this region of small solar impact distance.

B. Discussion of X-Band Scintillation Measurements

A cause of depressed or reduced scintillation-index value occurs when the signal traverses regions of less dense and less turbulent plasma, such as coronal holes. Most of the MGS 1998 X-band ingress points lie below the theoretical model depicted by the solid curves in Fig. 2 as the spacecraft signal was propagating through a coronal hole. The MGS 1998 egress measurements lie above and below the theoretical model, with data points lying above the model appearing to be correlated with solar activity [2].

Most of the temporal solar activity as detected in the spectral-broadening bandwidth measurements occurred during the Cassini May 2000 solar conjunction near the peak of the maximum of Solar Cycle 23. For the small SEP angles when the X-band was in saturation, changes in the scintillation index would not be observable. The resulting variations were detectable in the spectral-broadening bandwidth data, which do not saturate as the SEP angle decreases [2].

A significant increase in the X-band scintillation index was observed during a Cassini solar conjunction pass in May 2000 [3]. This event occurred during a pass conducted at an SEP angle of 1.8 deg during egress,
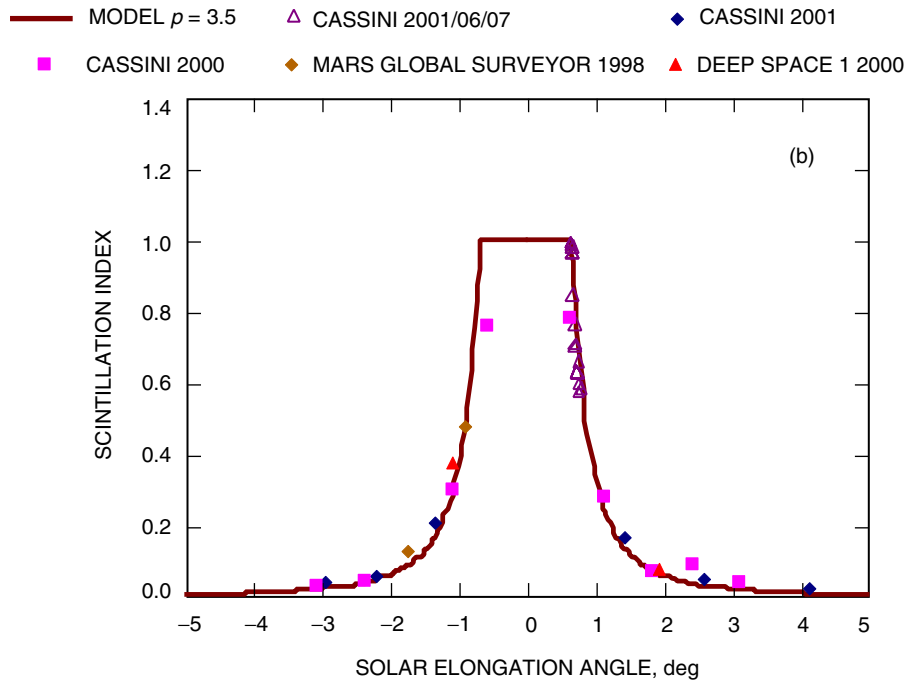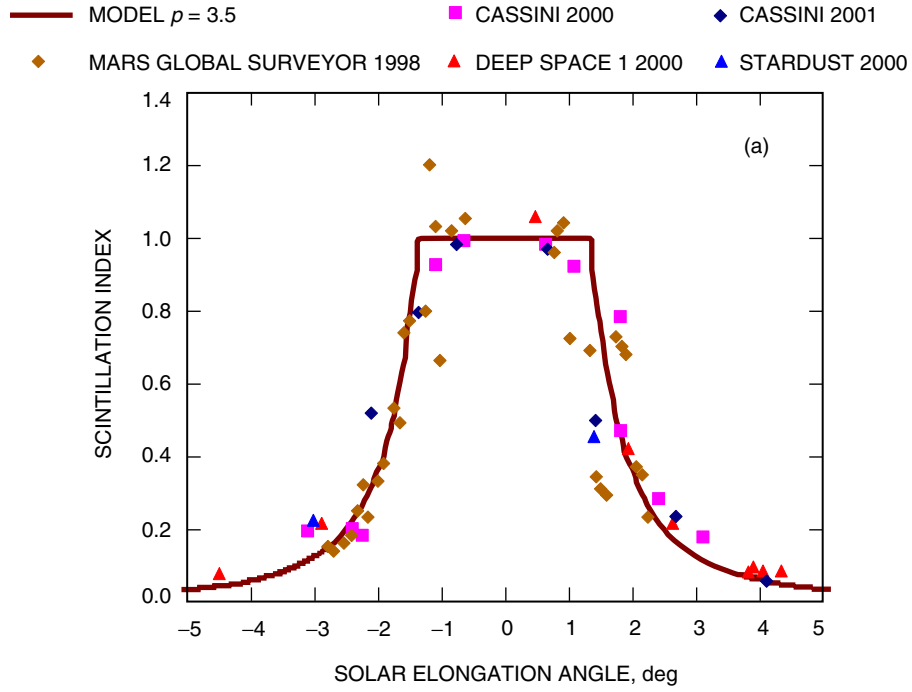
Fig. 2. Scintillation-index measurements from spacecraft solar conjunctions and theoretical models: (a) X-band and (b) Ka-band. The ingress is denoted by negative SEP angles, and egress is denoted by positive SEP angles.

while in the X-band weak-scintillation realm ($m < 1$). Hence, coronal electron-density-induced changes were detectable in which m increased from its background level of $m \sim 0.4$ up to $m \sim 0.8$. These two data points are plotted in Fig. 2(a). This change in the X-band scintillation index during a single pass is consistent with the overall scatter of all the measurements about the model for SEP < 2 deg, suggesting that such variability may contribute to the scatter seen in other measurements.

The solar-maximum scintillation observations of the Cassini 2000, Cassini 2001, and DS1 2000 solar conjunctions tend to be elevated with respect to the MGS 1998 data points, except during the solar events or streamer transits during egress, when there is reasonable agreement.

C. Discussion of Ka-Band Scintillation Measurements

The Ka-band scintillation measurements appear to be a reasonably good match to the theoretical model chosen (see Section III), as seen in Fig. 2(b). In addition to there being less scintillation at Ka-band relative to X-band for the same SEP angle, there is also less variability in the Ka-band scintillation index measurements, although it is cautioned to keep in mind that the Ka-band data set lacks a sufficient number of measurements. The Ka-band scintillation curve appears to transition from weak scintillation to saturation at an SEP angle near 0.6 deg.

A very few Ka-band data points were available from the MGS 1998 solar conjunction; thus, the Ka-band data set is not as comprehensive as that of the X-band. Changes in the Ka-band scintillation index during the Cassini May 2000 solar conjunction were difficult to measure, as the spacecraft was using thrusters to maintain pointing [3]. Thus, signal-amplitude excursions of as much as 20 dB occurred, with time scales on the order of 40 minutes. Thus, to minimize these effects for the Cassini May 2000 solar conjunction passes, the scintillation index for Ka-band was computed only during a short period of relatively constant signal strength, when dead-banding effects were minimal. The Cassini June 2001 solar conjunction had reaction wheel control, which resulted in excellent signal-strength stability; however, fewer solar transient events were observed during this solar conjunction.

D. Spectral-Broadening Data

Spectral broadening of the received carrier signal occurs due to Doppler shifting of the charged-particle refractive-index (or density) irregularities as they are carried over the signal path by the solar wind. The broadened bandwidth is calculated from power spectra computed from open-loop receiver data and is defined as the bandwidth for which half of the signal power resides. This parameter, B, is a function of both solar-wind velocity and electron-density irregularities, and it has a dependence on the power-law index, p, described in Section III. An independent method of evaluating the power-law index makes use of simultaneous dual-band spectral-broadening measurements. The ratio of the spectral-broadened bandwidth between two wavelengths is related to the power-law index, p, by

$$\frac{B_{Ka}}{B_X} = \left(\frac{\lambda_{Ka}}{\lambda_X}\right)^{2/(p-2)} \tag{1}$$

Using the nominal Ka-band-to-X-band wavelength ratio of 1/3.8, the value of p can be solved from the simultaneous broadened bandwidth measurements by rewriting Eq. (1) as

$$p = 2 + 2\frac{\log\left(\frac{\lambda_{Ka}}{\lambda_X}\right)}{\log\left(\frac{B_{Ka}}{B_X}\right)} \tag{2}$$

Figure 3 displays a plot of the spectral (power-law) index obtained from simultaneous X-band and Ka-band broadened bandwidth measurements from the Cassini 2000 solar conjunction. These data were acquired from only the Goldstone complex using the research and development beam-waveguide 34-m-diameter antenna, Deep Space Station (DSS) 13, and reflect SEP angles ranging from near 0.6 deg to about 3 deg. Each data point represents an estimate made over 400 seconds of open-loop-receiver samples using fast Fourier transforms (FFTs). In addition, the mean power-law exponent estimated over each pass also is plotted in Fig. 3. The power-law exponent, p, ranges from about 3.2 to just above 4, usually within each pass, and is consistent with the expected range of measured values (see Section III). The mean value of p estimated from all of the measurements in Fig. 3 is 3.51 ± 0.01 (error in the mean). Thus, a value of $p = 3.5$ appears reasonable as representative of solar coronal conditions during the Cassini 2000 solar conjunction and can be used in the theoretical model formulation to be discussed next in Section III.
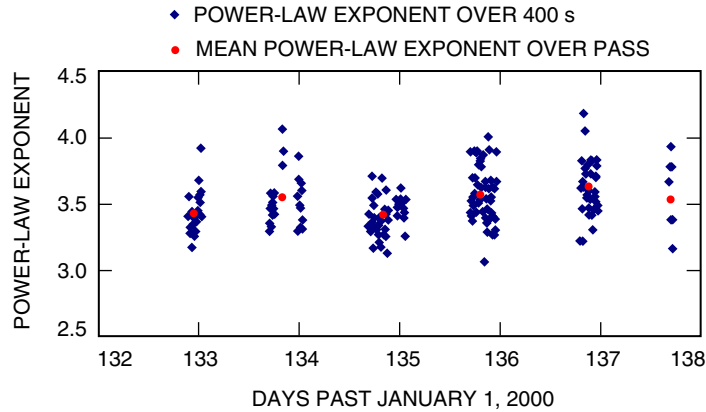

Fig. 3. Estimates of power-law exponent of three-dimensional spectrum of electron-density irregularities using simultaneous X-band and Ka-band spectral-broadening measurements from open-loop data recorded at Goldstone, DSS 13, during the Cassini May 2000 solar conjunction. The gaps reflect the fact that only one Deep Space Communications Complex was involved in data collection.

III. Theoretical Modeling of Amplitude Scintillation due to Solar Charged Particles

Figure 1 displays the relevant geometry of the Earth-to-spacecraft radio link relative to the Sun. This section will describe the theoretical model used and will closely follow the formulation given by Armstrong and Woo,[2] with detail from Marians [6], Ishumaru [7], and Rickett [8]. The model assumes that the signal emitted from a spacecraft is a monochromatic plane wave that propagates through many layers of charged particles in the solar corona and is received by a station on Earth. Each layer can be considered as a thin diffracting layer (or screen), for which a wavefront undergoes phase corrugations after passage through it. Individual points on the corrugated wavefront are considered to be independent radiators, each of which is considered a point source with a different phase. Here, only phase scintillation of the signal is observable. As the wave propagates further and reaches the observing station, an interference (or diffraction) pattern is formed at the Earth, observable as both amplitude and phase scintillation.

The function U is used in scattering theory and is often used to describe the strength of the fluctuations [7]. The equation used to represent U, the approximation to m^2, when $U << 1$ closely follows the notation of Ishimaru [7]:

---

[2] J. Armstrong and R. Woo, JPL Interoffice Memorandum 3331-80-070 (internal document), Jet Propulsion Laboratory, Pasadena, California, December 15, 1980.

$$U = r_e^2 \lambda^2 \int_0^L dl' C_N^2(q, z) \Gamma(p-1) \sin\left(\frac{\pi}{2}(p-3)\right) \left(\frac{2\pi}{\lambda z}\right)^{-(p-2)/2} \cos\left(\frac{\pi}{4}(2-p)\right) \Gamma\left(\frac{p-2}{2}\right) \qquad (3)$$

where

$r_e =$ classical electron radius, 2.82×10^{-15} m

$\lambda =$ the wavelength of the radio wave, m

$z =$ the effective screen distance given by $(L - l')l'/L$ (see Fig. 1)

$p =$ the power-law index of the refractive index fluctuation spectrum

$L =$ the total signal path distance (see Fig. 1)

$C_N^2 =$ the "level" of the charged-particle density perturbations (or strength of the turbulence)

$q =$ the spatial wave number

$l' =$ the distance from Earth to the element dl' in the signal path being integrated (see Fig. 1).

$\Gamma(\ ) =$ the Gamma function

The calculation of U in Eq. (3) allows the magnitude of amplitude scintillation to be predicted for different sets of assumptions. For weak scintillation, $U << 1$ and $U = m^2$; at the transition region from weak to strong scintillation, $U \approx 1$ and $m = 1$; and for saturation, $U >> 1$ and $m \to 1$, asymptotically. This holds for a point source like a spacecraft signal, but for sources with detectable angular extent, such as natural radio sources, once U reaches unity, m will fold back down towards zero as the SEP angle continues to decrease [6].

The formulation in Eq. (3) gives the appearance of mathematical artifacts such as a singularity, which results if a value of $p = 3$ is used. Equation (3) was derived to match the formulation and notation of Ishimaru [7].[3] An alternate formulation of Rickett [8] could be used to avoid the artifacts. For the treatment presented here, it will be assumed that the range of values considered for p is $3.2 < p < 4$, which does not present any problems with singularities, and thus the above formulation suffices.

The scattering model used in Eq. (3) assumes that the three-dimensional spectrum of the charged-particle (electron-density) irregularities, which in turn causes the signal amplitude fluctuations, is isotropic and a power law of the form

$$P_{3N}(q, l', p) = C_N^2(q, z) \frac{\Gamma(p-1) \sin\left(\frac{\pi}{2}(p-3)\right)}{4\pi^2} q^{-p} \qquad (4)$$

where p and l' are as given above, and the quantity q is the spatial wave number given by

$$q = \frac{2\pi}{\sqrt{\lambda z}}$$

It is accepted that $P_{3N}(q, l', p)$ as given in Eq. (4) obeys a power law with p as the exponent [6, references therein]. However, several different values have been assigned to p. Kolmogorov [9] predicted a value of $p = 11/3(3.67)$, while early spacecraft measurement experiments have yielded values ranging

---

[3] J. Armstrong, personal communication, Jet Propulsion Laboratory, Pasadena, California, January 2003.

from 3.12 to 4.17 [10]. Armstrong and Woo[4] measured values from spacecraft measurements predominately in the ecliptic, ranging from $p = 2.8$ to 3.4 close in to the Sun (<6 solar radii) and values of $p = 4$ and above further from the Sun (between 6 to 30 solar radii). The smaller value of $p = 3.2$ is indicative of flattening of the spectrum of the refractive-index irregularities near the Fresnel wave number, while $p = 11/3$ (3.67) is indicative of classical Kolmogorov turbulence. The assumption that the spectrum does not change appreciably with solar radii distance has been referred to as a "fixed p model." A variable p model would employ a scaling factor that factors C_N^2 changing dimensions as ray-path impact distance changes.

The level of charged-particle perturbations, C_N^2, is a function of the perturbation in electron density and does not depend only on ray-path distance from the Sun, but also on solar latitude, incidence of solar transient events, and phase of solar cycle. This is supported by the presence of scatter of the scintillation measurements about a fixed model, the observed elevation of the measured scintillation index above the model during transient events, and the observed suppression below the model during signal transit through coronal holes. Usually C_N^2 is modeled as the sum of several terms as a function of solar-impact distance raised to different powers. A typical model follows:

$$C_N^2 = a_1 \left(\frac{r}{R_0} \right)^{-\alpha} + b_1 \left(\frac{r}{R_0} \right)^{-7} \tag{5}$$

where R_0 is solar radius (692,000 km) and r is the signal ray path's distance to the Sun at the element dl' being integrated over in Eq. (3) (see Fig. 1).

It should be reemphasized that C_N^2 is a measure of the strength of "fluctuations" in electron density and is not a measure of electron density. Its numerical value can be adjusted by varying the coefficients a_1 and b_1. The first term in Eq. (5), with $\alpha \sim 4$, dominates at large solar radii distances while the second term in Eq. (5) dominates at small solar radii.

The electron-density perturbation models for solar plasma can be expressed not just as a function of solar distance, r, but also of solar latitude, θ. Another form of the model of Eq. (5) could include a functional dependence on solar latitude. However, the latitudinal dependence is neglected in this study, as solar transient activity appears to dominate the scatter of the scintillation measurements (see Section II).

The theoretical model for solar scintillation assumes the functional forms of Eqs. (3) through (5) and the integration described in Eq. (3) to determine the value of U for both X-band and Ka-band. The integration was numerically executed in steps of $dl' = 0.001$ au along the signal path from Earth to spacecraft (0 to L in Fig. 1). The values of L_1 and L_2 of the Cassini May 2000 solar-conjunction geometry were used for the theoretical model formulation. The geometries of the other solar conjunctions do not significantly affect the shape of the curves if all other parameters remain fixed.

The power-law index chosen for the theoretical model was $p = 3.5$ based on the results discussed in Subsection II.D, which falls within the measured range of power-law index values for ray-path impact distances within 15 solar radii, as demonstrated from numerous earlier spacecraft measurements.

The model of C_n^2 in Eq. (5) assumes the conventional planetary solar conjunction geometry shown in Fig. 1, with $a_1 = 0$ and b_1 adjusted until the model in Eq. (3) closely matched both X-band and Ka-band measurements presented in Section II. The decision to set $a_1 = 0$ and to adjust b_1 was made to simplify the "fitting" process (fewer parameters) and can be justified on the basis that the b_1 term in Eq. (5) dominates at very small SEP angles for which the measurements apply.

---

[4] J. Armstrong and R. Woo, op cit.

The scintillation index used for the theoretical curves versus SEP in Fig. 2 was computed by taking the square root of U, when $U < 1$, and was set equal to unity ($m = 1$) for values of $U \geq 1$. This was done for both X-band and Ka-band. There appears to be reasonable agreement between the models (red curves) and data using the above formulation and assumptions, with $a_1 = 0$ and $b_1 = 3.8 \times 10^{22}/m^3$.

There is a region where the X-band curve in Fig. 2 lies above the data in the cusp region of the curve (where the transition from $m < 1$ to $m = 1$ occurs). The curve could be refined to fit these data. However, deriving a theoretical model based on a single set of parameters (geometry, power-law exponent, scattering model coefficients) that matches both the X-band and Ka-band data requires significant complexity and is not feasible. Different solar conditions occur for the different solar conjunctions and even for measurements within the same conjunction (p changes, and the density fluctuation profile changes).

If the assumption is made that different values of p and different sets of coefficients can be used in Eq. (5) for both frequency bands, then separate curves can easily be derived that fit both data sets for different solar conjunctions. Solar latitudinal dependence and phase of solar cycle dependence have been neglected in the model because temporal solar variability effects appear to dominate at the small SEP angles, as has been observed in the individual data sets.

The theoretical model presented as solid curves in Fig. 2 for X-band and Ka-band assumes a consistent set of parameters for both bands (the power-law index and density-fluctuation model are the same). The scatter of the scintillation measurements about the theoretical solar model in Fig. 2 is of order 0.14 for X-band and is much smaller, of order 0.03, for Ka-band, although the Ka-band data are more scant. This model provides a reasonably consistent fit of both X-band and Ka-band data within 5 deg of the Sun, using the mean power-law index of 3.5 derived from spectral-broadening measurements, the Cassini 2000 geometry, and the adjusted b_1 coefficient of Eq. (5), neglecting sub-solar latitude and solar phase dependence. The scatter about this fit thus accounts for temporal, solar-phase, and solar-latitude variability of the observations. The scatter of the X-band data about the X-band curve is significantly higher than that of the Ka-band data about the Ka-band curve and interestingly has a ratio near that of the wavelength ratio between the two bands, but it should be borne in mind that the Ka-band data set is scant.

The process described above was applied to both X-band and Ka-band data sets, with the wavelength dependence as specified in Eq. (3) and with contributions from both turbulence, λ^2, and spatial wave number dependence, $\lambda^{(p-2)/2}$. In some cases, when the scintillation index of one frequency band is known at a given SEP angle, one can estimate the scintillation index at another frequency band without performing the full integration process. The Ka-band scintillation index, m_{Ka}, can be related to the X-band scintillation index, m_X, assuming weak scintillation, ($m = \sqrt{U}$), as

$$ \frac{m_{Ka}}{m_X} = \left(\frac{\lambda_{Ka}}{\lambda_X} \right)^{(2+p)/4} \tag{6} $$

where p is the power-law index as previously described. Given a wavelength ratio of $\lambda_X/\lambda_{Ka} = 3.8$, then $m_{Ka}/m_X \sim 0.15$ for Kolmogorov turbulence ($p = 11/3$), and $m_{Ka}/m_X \sim 0.16$ for the case of $p = 3.5$.

IV. Fitting Solar Scintillation-Index Measurements to an Analytic Model

For purposes of engineering predictions, flight project planning, or post-pass comparison with measurements, it is desirable to have a quick "cookbook" method of estimating the scintillation index for a given SEP angle or SEP angle range in lieu of the more rigorous theoretical model method described in Section III. The scintillation index at a given SEP angle can be estimated using an analytic model as a

function of SEP angle. A combination polynomial/exponential model was chosen and independently fit to the X-band and Ka-band measurements over the SEP angle range of the measurements depicted in Fig. 2.

For convenience of fit, both ingress and egress data were combined so that the SEP angle used for the fit is its absolute value. The assumption is made that all of the solar effects over the long term are isotropic, so that the scatter about the fit should represent short-term variability due to solar transient events and the spatial differences in coronal density fluctuations often reflected in asymmetry of ingress and egress data sets. Thus, the rms scatter of m as a function of SEP angle about the nominal fitted analytic curve can be inspected to infer a range of the variation of the scintillation index.

A combination exponential/polynomial model of the following form was fit to the measurements:

$$m = \exp\big(-a_1(\theta - \theta_t)\big) + a_2 + a_3(\theta - \theta_t) + a_4(\theta - \theta_t)^2 \tag{7}$$

where a_1, a_2, a_3, and a_4 are solve-for coefficients and θ_t is the SEP angle at the transition point from weak scintillation ($m < 1$) to saturation ($m = 1$), which was chosen to be 1.1 deg for X-band and 0.6 deg for Ka-band. The first set of model fits to the data using Eq. (7) included all of the spacecraft scintillation measurements with $\theta_t < \theta$, where the model is constrained to be unity for $\theta_t > \theta$.

For X-band, the best-fit coefficients using the exponential model in Eq. (7) fit to the data with an SEP angle above 1.1 deg were

$$a_1 = 1.14 \pm 0.09$$

$$a_2 = 0 \text{ (fixed)}$$

$$a_3 = 0.02 \pm 0.02$$

$$a_4 = 0 \text{ (fixed)}$$

where $\theta_t = 1.1$ deg for 1.1 deg $< \theta <$ 5 deg.

For Ka-band, the best-fit coefficients using the exponential model in Eq. (7) were

$$a_1 = 1.50 \pm 0.09$$

$$a_2 = -0.231 \pm 0.024$$

$$a_3 = 0.176 \pm 0.024$$

$$a_4 = -0.030 \pm 0.009$$

where $\theta_t = 0.6$ deg for 0.7 deg $< \theta <$ 5 deg.

The exponential/polynomial model-fitted curves as well as the measurement data are shown in Fig. 4 for both X-band and Ka-band. For additional insight, X-band scintillation-index measurements of a natural radio source also are included [11]. The natural radio source data are in good agreement with the spacecraft data and the model curve plotted in Fig. 4.
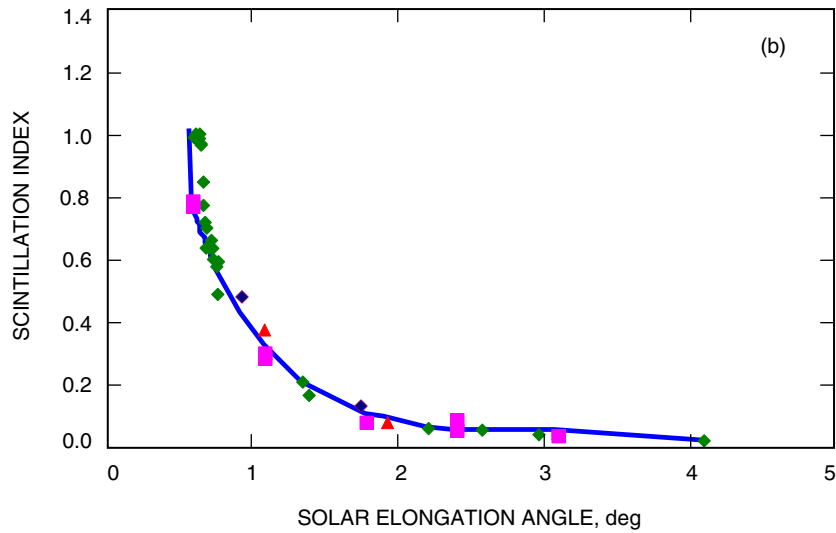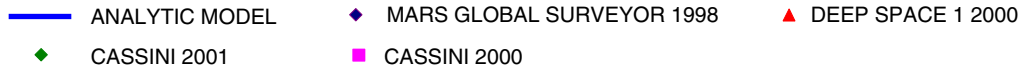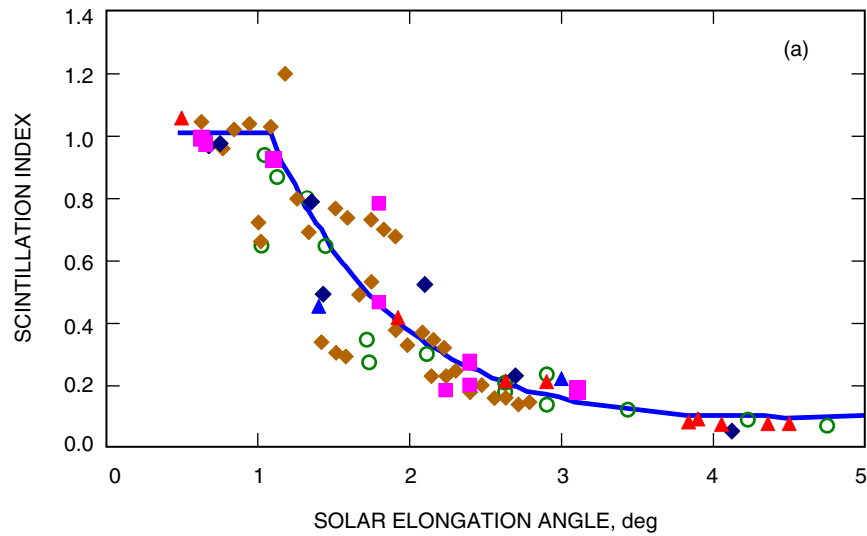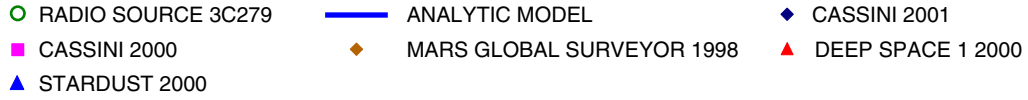
Fig. 4. Scintillation-index measurements from spacecraft solar conjunctions and natural radio source data, along with analytic model curves, which were fit to the spacecraft data as described in the text: (a) X-band and (b) Ka-band.

The rms scatter of the data to the analytic model is of reasonable quality, ≈ 0.13 for X-band and ≈ 0.03 for Ka-band. There is significant scatter of the X-band measurements for solar elongation angles within 2 deg. The X-band fitted curve lies above most measurements for SEP angles between 2 deg and 3 deg. However, most of the data points that lie below the curve in this region are from the MGS 1998 solar conjunction during ingress transit of the received signal through a coronal hole.

A separate fit of the model in Eq. (7) was performed for only the X-band measurements for SEP angles above 2 deg, with resulting best-fit coefficients of

$$a_1 = 1.74 \pm 0.45$$

$$a_2 = 0.186 \pm 0.184$$

$$a_3 = -0.036 \pm 0.060$$

$$a_4 = 0 \text{ (fixed)}$$

where $\theta_t = 1.1$ deg and 2 deg $< \theta <$ 5 deg.

The resulting model curve for X-band, which was fit only to the weak scintillation data with SEP $>$ 2 deg, resulted in a much smaller scatter of $\approx$0.06, which is comparable to that of the Ka-band data about the fit model down to SEP $>$ 0.6 deg (near Ka-band saturation). The extrapolation of this X-band model to SEP angles below 2 deg does not pass through the data points located in the transition region between 1.1 deg and 2 deg, but instead lies mostly above it. With the constraint reflected in the setting of the parameter $\theta_t = 1.1$ deg, the model curve slices almost midway through the data points from an SEP angle of 2 deg to about 1.5 deg, then lies significantly above the data points from 1.5 deg down to the saturation transit point at $\theta_t = 1.1$ deg. It is cautioned that the coefficients from this limited SEP angle fit be used only for SEP angles above 2 deg for X-band, and that the previous fit coefficients reflected in the X-band curve in Fig. 4 be used for SEP $<$ 2 deg with cognizance of the increased scatter of the data about the fitted curve in this region.

For SEP $<$ 2 deg, there is a region of significant variability or scatter of the X-band data about the model, regardless of the fit. The scatter is significantly higher in the region of transition from weak to strong scintillation (2 deg $>$ SEP $>$ 1.1 deg). The occurrence of solar transient events in the signal path can significantly elevate the measured scintillation index (during coronal mass ejections, for example) or significantly depress the value (during signal transit through coronal holes). The magnitude of the scatter in scintillation will be greater as the SEP angle decreases until saturation is reached. It is cautioned that many more observations over a wide range of solar conditions are required in order to realize a better characterization of variability in the scintillation index.

V. Conclusion

Theoretical and statistical models for solar-scintillation index as a function of solar elongation were presented. These models were based on signal-amplitude measurements acquired from different space-craft superior solar conjunctions at both X-band and Ka-band. A theoretical model was presented that simultaneously fit both X-band and Ka-band data sets using the same geometry, spectral power-law index, and scattering model parameters. A combination exponential/polynomial statistical model was fit to each data set. The scatter of the measurements about the models represents variability, which may be due to occurrence of solar transient events, variation with phase of solar cycle, or sub-solar latitude. The derived statistical models for X-band result in a very low rms scatter about the fit for data with SEP angles above 2 deg. There is significantly higher scatter of the X-band measurements about a fit in the transition region between an SEP angle of 1.1 deg and 2 deg. The SEP angle near 2 deg appears to be a transition boundary when telemetry frame errors are significant for $\theta < 2$ deg and much improved for $\theta > 2$ deg [1]. However, the Ka-band fitted curve follows the model very well down to 0.6 deg near saturation, with very low rms scatter. Nevertheless, the paucity of the Ka-band measurements should be taken into consideration, and additional measurements should be acquired to supplement this data set in order to better characterize solar scintillation effects at Ka-band.

These models will be useful for setting up and conducting future solar conjunction operational scenarios and can be refined as more measurements from future solar conjunctions are combined into the data sets. The upcoming Mars Reconnaissance Orbiter (MRO) mission will have simultaneous X-band and Ka-band downlink channels, which will allow for further characterization of carrier-signal fluctuations as well as telemetry channel data for both frequency bands in which the measured frame errors can be correlated against measured scintillation index and the derived models. Thus, telemetry performance for X-band and Ka-band can be inter-compared and compared against theoretical and statistical predictions. The models can be refined further as a function of solar elongation angle and perhaps as a function of other parameters such as solar cycle phase and sub-solar latitude.

Acknowledgments

References

[1] D. D. Morabito and R. Hastrup, "Communicating with Mars During Periods of Solar Conjunction," *Proceedings of the 2002 IEEE Aerospace Conference,* Paper 103, Big Sky, Montana, March 9–16, 2002.

[2] D. Morabito, S. Shambayati, S. Butman, D. Fort, and S. Finley, "The 1998 Mars Global Surveyor Solar Corona Experiment," *The Telecommunications and Mission Operations Progress Report 42-142, April–June 2000,* Jet Propulsion Laboratory, Pasadena, California, pp. 1–18, August 15, 2000.
http://tmo.jpl.nasa.gov/tmo/progress_report/42-142/142C.pdf

[3] D. D. Morabito, S. Shambayati, S. Finley, and D. Fort, "The Cassini May 2000 Solar Conjunction," *IEEE Transactions on Antennas and Propagation,* vol. 51, no. 2, pp. 201–219, February 2003.

[4] D. D. Morabito, S. Shambayati, S. Finley, D. Fort, J. Taylor, and K. Moyd, "Ka-band and X-band Observations of the Solar Corona Acquired During Solar Conjunctions of Interplanetary Spacecraft," *Proceedings of the 7th Ka-band Utilization Conference,* Santa Margherita Ligure, Istituto Internazionale delle Communicazioni, Genova, Italy, September 26, 2001.

[5] Y. Feria, M. Belongie, T. McPheeters, and H. Tan, "Solar Scintillation Effects on Telecommunication Links at Ka-Band and X-Band," *The Telecommunications and Data Acquisition Progress Report 42-129, January–March 1997,* Jet Propulsion Laboratory, Pasadena, California, pp. 1–11, May 15, 1997.
http://tmo.jpl.nasa.gov/tmo/progress_report/42-129/129A.pdf

[6] M. Marians, *Theory of Scintillations Due to Propagation Through a Turbulent Medium,* Ph.D. Dissertation, University of California, San Diego, 1975.

[7] A. Ishimaru, *Wave Propagation and Scattering in Random Media,* vol. 2, New York: Academic Press, 1978.

[8] B. J. Rickett, "Interstellar Scattering and Scintillation of Radio Waves," *Ann. Rev. Astr. Astrophys.,* eds. G. Burbidge, D. Layzer, and J. Phillips, vol. 15, pp. 479–504, Annual Reviews Inc., Palo Alto, California, 1977.

[9] A. N. Kolmogorov, *Doklady Akademii Nauk,* USSR, 32, p. 16, 1941.

[10] T. W. J. Unti, M. Neugebauer, and B. E. Goldstein, "Direct Measurements of Solar Wind Fluctuations Between 0.0048 and 13.3 Hz," *Astrophysical Journal,* vol. 180, no. 2, pp. 591–598, 1973.

[11] W. A. Coles, "Inter-Planetary Scintillation," *Space Science Rev.,* vol. 21, no. 4, pp. 411–425, 1978.